IEEE ROBOTICS AND AUTOMATION LETTERS. PREPRINT VERSION. ACCEPTED JANUARY, 2026

3D-Printed Volume Adjustable Socket for Above-Knee Prostheses

Federico Donadel, Ahmed Z. Zaidi, Arianna Menciassi, *Fellow, IEEE*, Linda Paternò, *Member, IEEE*

***Abstract*—Traditional prosthetic sockets are rigid, passive structures that cannot accommodate daily residual limb volume fluctuations and are produced through labor-intensive processes involving environmentally and occupationally hazardous materials. This work presents a 3D-printed, volume-adjustable transfemoral socket integrating a motorized cable-driven mechanism and pressure monitoring. The design features a dual-layer, concentric structure that enables uniform circumferential modulation via a BOA® system, operable manually or through a DC motor. Four resistive sensors, embedded in a prosthetic liner with a magnetic suspension, provide interface pressure feedback for closed-loop control. The socket is fabricated using 3D-printed glass-filled PA12 and carbon-fiber-reinforced PEEK to optimize strength, weight, and reduce material waste by means of a more sustainable production process. Experimental validation showed that the system maintains interface pressure within the target range (70 ± 2 kPa), limits relative vertical displacement down to <6 mm under realistic tension load, and withstands static and dynamic forces up to 900 N without structural failure. This solution combines adaptive design with sustainable digital manufacturing, offering a robust foundation for next-generation wearable physical interfaces that enhance comfort and stability.**

***Index Terms*— Wearable robotics, prosthetics and exoskeletons, actuation and joint mechanisms, adaptive socket, residual limb volume fluctuation.**

I. INTRODUCTION

Over 57 million people worldwide are living with limb loss, with lower limb amputations accounting for approximately 85% of all cases [1]. For these individuals, prosthetic limbs are essential tools for restoring mobility and supporting a return to independent, active lives. Among the various components of a prosthesis, the physical interface between the user's residual limb and the prosthetic device is a fundamental factor in determining the overall effectiveness. This interface, known as socket, is typically a rigid, passive component custom-molded to the user's anatomy and often combined with a silicone prosthetic liner to improve comfort and increase friction, thus ensuring better grip and stability [2].

One of the main limitations of traditional sockets is their inability to accommodate daily physiological changes in residual limb volume, which can fluctuate by approximately −11% to +7% throughout the day [3], [4]. These fluctuations alter the socket fit and can lead to uneven pressure distribution on tissues, discomfort, and skin complications [5]. Thus, various adjustable socket systems have been proposed in literature and on the market. As reported in Baldock et al. [6], these systems can be broadly categorized into three main groups: (*i*) pneumatic bladder-based systems, which use pressurized air to inflate soft chambers within the socket and modulate local interface pressure, but are prone to mechanical failure and require bulky, noisy pumps [7]-[9]; (*ii*) modular panel-based systems, which incorporate floating or hinged elements into the socket wall to enable localized volume adjustment, but offer only limited movement of discrete sections, resulting in uneven pressure distribution on tissues and often requiring complex fabrication processes [10]; and (*iii*) circumferential adjustment systems, the most widely adopted in clinical practice, which adapt the socket to residual limb volume changes by uniformly regulating its circumference through deformable struts combined with straps, ratchets, or cable-driven mechanisms, [11]. These latter systems achieve global socket deformation, ensuring more uniform pressure distribution and improved comfort and stability.

Notable examples of circumferential adjustment systems on the market include Ottobock Varos [12], and Ossür Connect TF [13]. Although mechanically robust, these solutions are prefabricated sockets, not personalized on the user's residual limb shape. Consequently, they are mainly recommended for the early phase after amputation [14], when volume changes range approximately from -35% to -10% [15]. Additionally, they are passive structures, requiring the user to manually intervene to maintain fit and not offering real-time control or feedback. This often leads users to apply excessive tightening to improve perceived stability, which may induce elevated pressures on tissues and, over time, exacerbate residual limb volume loss due to compromised circulation and mechanical compression. In addition to these functional drawbacks, traditional socket fabrication methods also pose practical and environmental challenges. Most sockets are fabricated through a resin lamination process, in which carbon fiber or fiberglass layers are applied over a cast of the residual limb and impregnated with epoxy resin. This multi-step process is labor-intensive, time-consuming, and costly. Moreover, it poses health risks to technicians and has a significant environmental impact due to the use of non-recyclable composites and toxic chemicals, which can release harmful dust and volatile

Manuscript received: August 6, 2025; Revised: October 26, 2025; Accepted: January 14, 2026.

This paper was recommended for publication by Editor Haoyong Yu upon evaluation of the Associate Editor and Reviewers comments.

This work was promoted by INAIL, the Italian National Institute for Insurance against Work-related Injuries (non-commercial entity), within the PR23-PAI-P2 eLiner project framework.

The authors are with the BioRobotics Institute, Sant'Anna School of Advanced Studies, 56127 Pisa, Italy (e-mail: federico.donadel@santannapisa.it; ahmedzohaib.zaidi@santannapisa.it; arianna.menciassi@santannapisa.it; linda.paterno@santannapisa.it).

Digital Object Identifier (DOI): see top of this page.

compounds during processing. In this regard, additive manufacturing (AM) is emerging as a promising alternative, enabling faster and lower-cost fabrication, and the ability to easily produce complex, patient-specific geometries without the need for multi-step lamination processes [16]. 3D printing supports a more sustainable and eco-conscious design approach by enabling precise material usage that minimizes waste, optimizing structures for lightweight and efficient resource consumption, and promoting localized production.

Thanks to recent advancements in materials and AM techniques, early examples of 3D-printed sockets designed to meet the mechanical and structural requirements of prosthetic use have been reported in literature. Specifically, 3D printing technologies such as fused deposition modeling (FDM), selective laser sintering (SLS), and multi jet fusion (MJF) have been applied using polymers like polyamide 12 (PA12/ nylon), PEEK, and high-performance composites such as carbon- or glass-fiber-reinforced polymers [17-20]. Notable examples include a PLA-based transtibial socket [17] and a PETG carbon-reinforced transtibial socket [21], both of which withstood ISO P6 load levels. In contrast, for transfemoral applications, the only case found in literature is a socket developed by Marinopoulos et al. [22], specifically for pediatric patients. Building on the reported unmet needs, this work presents a 3D-printed, circumferentially adjustable socket that integrates active components to enable volume regulation (Fig. 1). The system allows for circumference modulation either manually using a BOA® dial [23], or automatically via a DC motor connected to the dial and operating in open- or closed-loop mode, based on pressure feedback from sensors embedded in the liner and accessible via a mobile application. This design combines pressure monitoring with adaptive design, enabling users to make informed, responsive modifications to optimize fit and comfort. AM supports a customizable and sustainable fabrication process, promoting patient-specific design.

II. Materials and Methods

A. Adjustable Socket System

The proposed socket is a cable-driven adjustable structure consisting of two concentric layers, where the external layer slides smoothly over the internal one, enabling circumference modulation while maintaining continuous, total contact with the residual limb tissues (Fig. 1). To achieve customized fit and ensure even pressure distribution, the two layers were shaped based on a 3D scan of a high-fidelity, transfemoral residual limb simulator, which was used for final socket validation. This approach was chosen to enable a systematic characterization under controlled, repeatable conditions. Residual limb volume changes are mainly driven by body fluid dynamics, influenced by a complex interplay of factors such as physiological and biometric characteristics. This variability makes consistent and effective evaluation in human subjects particularly challenging.

Socket volume is modulated by tightening or loosening a steel cable (BOA® CS1; 7×7 strand; diameter: 0.9 mm; total length: 1150 mm, covered with nylon), routed through fourteen low-friction BOA® cable guides positioned at 2.5 cm intervals along the length of the socket on the lateral side (Fig. 1d). This configuration and number of guides were selected considering the dimensions of both the guides and the socket, ensuring uniform circumferential tightening along the socket length while minimizing actuation load to tension the cable. Cable tension is controlled via a BOA® Li2 dial (diameter: 28.3 mm; height: 13 mm), that rotates counterclockwise (CCW) to loosen and clockwise (CW) to tighten the cable-driven mechanism simply rotating a knob, providing precise and even adjustment.

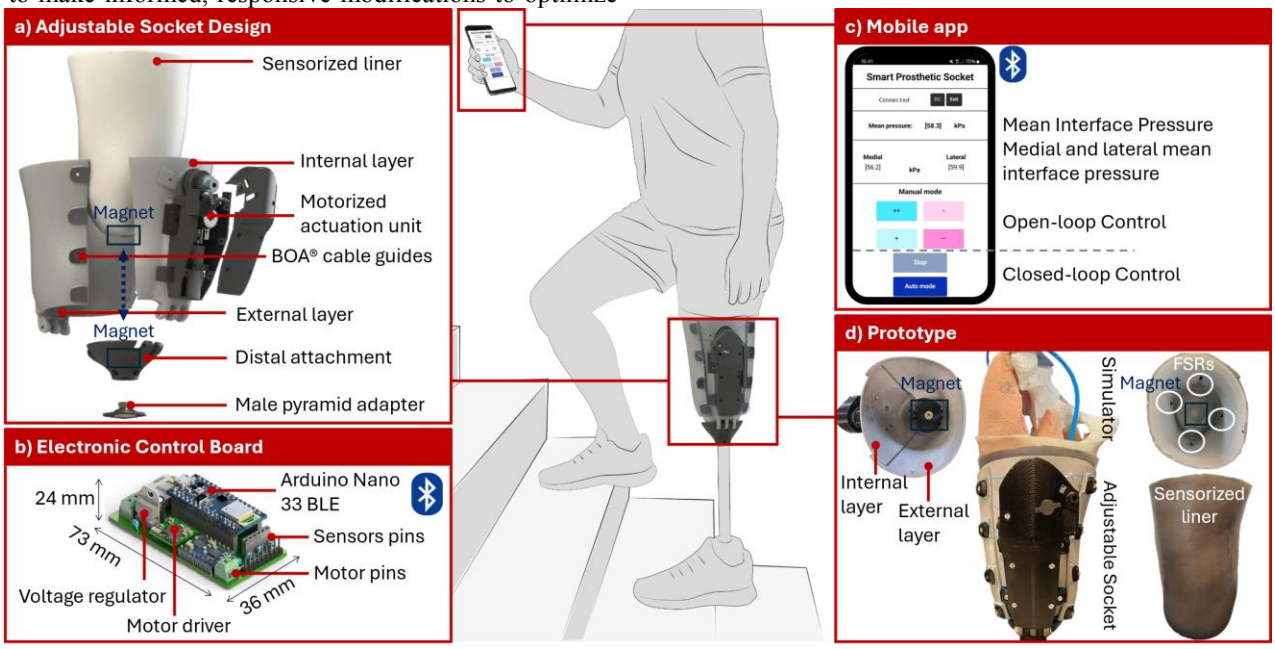

Fig. 1. (a) Exploded view of the circumferential adjustment socket, composed of two concentric layers connected via rotational joints to a custom distal attachment with an integrated magnet for magnetic suspension with the sensorized liner. A motorized BOA® cable system regulates socket circumference. The distal attachment includes a female pyramid adapter compatible with standard male components. (b) Electronic control board based on Arduino Nano 33 BLE (Bluetooth Low Energy). (c) Mobile app for pressure monitoring and control of the motorized unit in open- or closed-loop mode. (d) Top and lateral views of the final prototype of the assembled socket with the sensorized liner, mounted on the high-fidelity residual limb simulator. FSRs: Force-Sensitive Resistors.

This article has been accepted for publication in IEEE Robotics and Automation Letters. This is the author's version which has not been fully edited and content may change prior to final publication. Citation information: DOI 10.1109/LRA.2026.3662558

TABLE I. Properties of 3D printable materials for the distal attachment. PEEKCA20 was ultimately selected and validated through FEM simulations. The figure shows Von Mises stress distribution under a 4500 N load. The stresses remain well below the PEEKCA20 yield strength (55 MPa), confirming structural safety. Impact resistance refers to Izod tests. EX: excellent; G: good; D: difficult; VD: very difficult.

	PEEK	PEEKCA20	PEEKCA30	ULTEM1010	Ti
Density [g/cm3]	1.3	1.4	1.5	1.3	4.4
Tensile strength [MPa]	100	120 – 140	150 – 170	90	1000
Elastic modulus [GPa]	3.7 – 4	7	8.5 -10	3	110
Elongation at break [%]	30 - 50	2.5 - 5	1.5 - 3	5-30	10-15
Impact resistance [J/m]	80 – 100	60 – 80	50 - 70	50 - 70	100 - 150
Fatigue resistance	EX	EX	EX	G	EX
3D printability	D	VD	VD	D	D
Cost [€ /kg]	500 – 700	700 – 900	800 - 1000	300 - 500	400 - 800

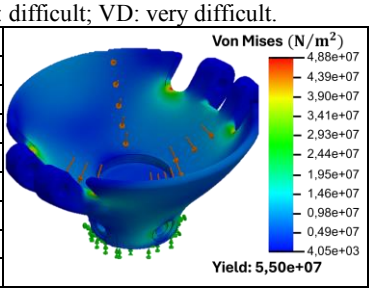

The dial can be rotated either manually or via a motorized mechanism thanks to a mechanical engagement integrated into the actuation unit that enables seamless switching between the two modes (Supplementary Video). The entire control unit, including the dial, DC motor, and gear transmission, is mounted on the external surface of the internal layer to minimize bulk and preserve compactness. The two socket layers are connected via a dual-pin rotational joint to a distal custom attachment, designed to structurally link the socket to standard prosthetic components through a standard female pyramid adapter.

Material selection for the 3D-printed socket was based on both literature evidence and mechanical simulations. For the socket concentric layers, carbon-reinforced nylon (PA12 CF) and glass-filled nylon (PA12 GB) were evaluated. While PA12 CF offers higher stiffness [18], PA12 GB was selected in collaboration with the printing provider [24] due to its superior impact resistance, lower anisotropy, and better dimensional stability, making it more suitable for dynamic, multi-axial loading of prosthetic use. The socket was 3D-printed via MJF approach. For the distal attachment, titanium (Ti), PEEK, PEEK with carbon reinforcement at 20% (PEEK CA20) and 30% (PEEK CA30), ULTEM 1010, and AISI 4340 steel were investigated (Table I). Among them, PEEK CA20 printed via FDM offered the best compromise between stiffness, fatigue resistance, and low density. PEEK is a high-performance thermoplastic material widely used in biomedical applications for its biocompatibility and chemical stability [25], [26].

To validate the material for the distal attachment, FEM simulations were performed in SolidWorks for all candidates by applying a 4.5 kN load to the conical inner surface, while constraining the component at its base to replicate the fixed connection to the prosthetic knee. This load is the ultimate static force that prosthetic components must withstand without failure, in accordance with ISO 10328 standard, P6 level (i.e., individuals with high mobility). The model assumed a linear-elastic isotropic behavior for PEEKCA20 (Elastic modulus = 7 GPa, Poisson module = 0.35, yield strength = 55 MPa). The mesh, generated with a curvature-based algorithm, consisted of approximately 81,000 nodes and 50,000 solid elements, with sizes ranging from 0.38 to 4.19 mm. Von Mises stress, equivalent strain, and factor of safety (FOS) were evaluated, confirming the material stress of PEEKCA20 well below its yield strength of 55 MPa, and a FOS equal to 2 (Table I). Among simulated materials, PEEKCA20 demonstrated superior mechanical performance compared to all alternatives except for titanium, which showed comparable stress and safety values but a significantly higher weight.

To enhance comfort, reduce vertical displacement, and maintain residual limb alignment, the socket is combined with a custom silicone liner with a magnetic suspension system. The liner was made of EcoFlex0050 silicone (Shore hardness: 00-50; Smooth-On Inc.), using a 3D-printed mold based on the 3D scan of the residual limb simulator. A neodymium (NdFeB) cylindrical magnet (diameter: 34 mm; thickness 4 mm; type N35; axial magnetization) was embedded distally in the liner, while a textile sock impregnated with silicone was applied to the external surface during polymerization to form a reinforced outer layer. The embedded magnet is paired with a corresponding magnet in the socket's distal attachment (Fig. 1a, c). For magnet selection, COMSOL simulations were conducted using the Magnetic Fields interface to evaluate the attractive force between the two magnets, modeled with manufacturer-specified material properties, including a remanent flux density corresponding to a nominal pull force of 98.1 N and a tangential force of 19.6 N. Simulations aimed to identify a magnet spacing that ensures stable coupling while maintaining the 10 N detachment force [27], recommended to prevent excessive user's effort during liner removal from the socket. The analysis focused on the axial force component while the center-to-center distance between the magnets was varied from 2 mm to 11 mm. Results indicated that a 5 mm spacing between the magnets yields 13.4 N attractive force, providing an effective trade-off between minimizing vertical displacement and allowing easy socket doffing. The liner also integrates four commercial FSR (Force-Sensitive Resistor) sensors (Ohmite FSR03) with an active sensing area of 25.42 mm diameter on a 0.425 mm thick film, embedded at key anatomical sites (anterior, posterior, medial, and lateral) to monitor interface pressure [28]. The sensors were calibrated using an Instron Machine, applying pressure from 0 to 150 kPa, typical interface pressure range in above-knee sockets [29]. The output voltage was recorded, and a reverse calibration curve was obtained for each sensor mapping the output voltage to the corresponding pressure. Sensors feature a detection sensitivity below 0.19 kPa (evaluated from the slope of the 0-20 kPa initial portion of the calibration curve, where the sensor response is most linear and less affected by hysteresis), a pressure resolution of approximately ±1 kPa (computed as the minimum detectable pressure variation), less than 1% drift, and mean single-unit repeatability of 2%. Although the sensors exhibit limited linearity (mean = 30.2 ± 20.7 kPa) and relatively high hysteresis (mean = 14.9 ± 5.9 kPa), their overall performance is acceptable for validating the system, being operated within a consistent mechanical configuration.

B. Motorized Actuation Unit

To automatically control the cable length, a Faulhaber 2342 DC motor coupled with a GPT22 planetary gearbox was selected for its high efficiency (80%) and precise control (Fig. 2). The motor operates at 12 V, delivers a nominal torque of 17 mNm, and reaches a no-load speed of 8100 rpm. When paired with the GPT22 planetary gearbox, the system achieves an output torque of up to 0.8 Nm (T_G). The motor with the gearbox measures 66.5 mm in length, 22 mm in diameter, and weighs 146 g, making it well-suited for integration into the prosthetic system. To further amplify the torque, a worm gear with a 1:30 reduction ratio (N_w/N_G) is connected to the GPT22 planetary gearbox and drives a worm wheel. Assuming 70% transmission efficiency, the output torque is evaluated as:

$$T_W = \frac{N_G}{N_W} \times T_G \times 0.7 \; = \; 16.8\, Nm \qquad (1)$$

Where N_G and N_w are the number of threads on the worm gear and the number of teeth on the worm wheel, respectively, and T_G and T_W are the corresponding torques. The T_W torque is then transferred to the BOA® dial via a three-stage spur gear transmission (module 1 mm; 30 teeth; 1:1 gear ratio). Gear 1 is rigidly connected to the worm wheel, and Gear 2 transfers the torque from Gear 1 to Gear 3, which is rigidly connected to the BOA® dial. Assuming 90% transmission efficiency, the torque transferred to the BOA® dial is 13.60 Nm, satisfying the 10 Nm target value specified by the manufacturer for effective cable tightening, thus ensuring reliable operation under all conditions. A transmission efficiency of 70% for the worm gear and 90% for the spur gears was assumed, reflecting the higher sliding friction of worm gears versus the rolling contact of spur gears.

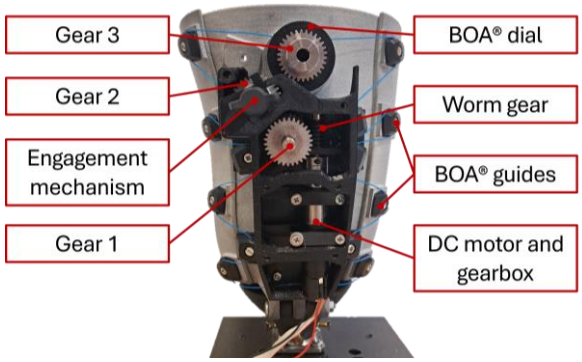

Fig. 2. Motorized actuation unit. The system integrates a DC motor with gearbox, a worm gear and worm wheel for torque amplification, and a three-stage spur gear transmission (Gears 1–3) that transfers torque to the BOA® dial. An engagement mechanism allows switching between motorized and manual operation.

The maximum cable tension force generated by the BOA® dial is then estimated to be equal to 486 N. The complete actuation unit weighs 587 g, with the gear train, comprising a worm gear and three spur gears, accounting for approximately 441 g. The proposed configuration was selected to ensure efficient force transmission while allowing the integration of the engagement mechanism that enables quick switching between motorized and manual control modes, providing manual override for safety. Specifically, the engagement mechanism includes Gear 2, mounted on a laterally movable shaft that can engage or disengage from Gear 3. When disengaged, torque transfer to the BOA® dial is interrupted, enabling manual adjustment of the dial itself. When engaged, motor torque is transferred to the BOA® dial, guaranteeing automatic control. A locking beam secures the shaft in both positions. To house and align the components, a dedicated PETG 3D-printed case was designed, consisting of a base fixed to the outer surface of the internal socket layer and a removable cover. The case (275g) supports motor and gear alignment and houses the engagement system.

An electronic control board connected to a 10.8 V, 3500 mAh Li-Ion rechargeable battery was developed to read interface pressures and to control the motor in both open- and closed-loop modes (total weight ~ 330g). The circuit consists of a microcontroller (Arduino Nano 33 BLE), a motor driver (Pololu - Motoron MT256) and two voltage regulators (LM340T-5 & U3V40F12) (Fig. 1b). Based on the system's current consumption, measured as ~300 mA during cable tightening (i.e., the most power-demanding phase) and about 200 mA during cable loosening, as experimentally determined over three repeated tests for each condition, the backup time was estimated assuming a constant current draw of 300 mA. This conservative assumption resulted in an estimated backup time of approximately 11 h 40 min under continuous operation. Thus, assuming up to 10 activations per day, each lasting approximately 2 min, the proposed configuration allows for up to 4 weeks of operation on a single charge, leaving ample margin to support a higher number of daily activations or continuous pressure monitoring. Assuming up to 10 activations per day, each lasting 2 min, the proposed configuration allows for up to 4 weeks of operation on a single charge, leaving ample margin to support a higher number of daily activations or continuous pressure monitoring. Indeed, it is worth noting that the actuation is obviously the primary contributor to power consumption, while sensors draw minimal current.

A customized mobile app was designed in the MIT App inventor to display pressure data and control the motor via Bluetooth Low Energy (BLE) communication standard (Fig. 1c). When the system is activated, and the app is connected to the board, the app displays the Mean Interface Pressure (MIP) from four FSR sensors, and the mean pressures from the medial and lateral sensor pairs, at a sampling rate of 5 Hz. A finite-state machine algorithm manages system functions in both open- and closed-loop modes (Fig. 3). Each button press on the app sends a switch state to the circuit, triggering a set of condition checks. In open-loop mode, the user can adjust the socket volume using four control buttons: ++ and + drive the motor CW at two different speeds to release the socket, while -- and - drive it CCW to tighten it. The *Stop* button can be used to stop the motor and exit the open-loop mode. When automatic mode is activated, a hybrid control strategy (a PI controller and an on-off mechanism) adjusts the socket volume in a closed-loop mode to maintain MIP around the 70 kPa ± 2 kPa target value, identified in clinical literature as suitable for standing position [29]. However, this threshold can be easily modified in the control software, enabling rapid customization for different users. Based on feedback collected through focus groups with

users and clinicians, the system is intended for intermittent use, with adjustments performed while the user is standing in a stable posture. In this configuration, the axial load does not interfere with the lateral cable-driven mechanism, preventing potential malfunction risk (Supplementary Video). The proposed approach allows the user to activate automatic regulation as needed or upon donning the prosthesis, and deactivate it once the desired fit is achieved, thereby avoiding the less safe continuous motor operation during walking and reducing overall power consumption.

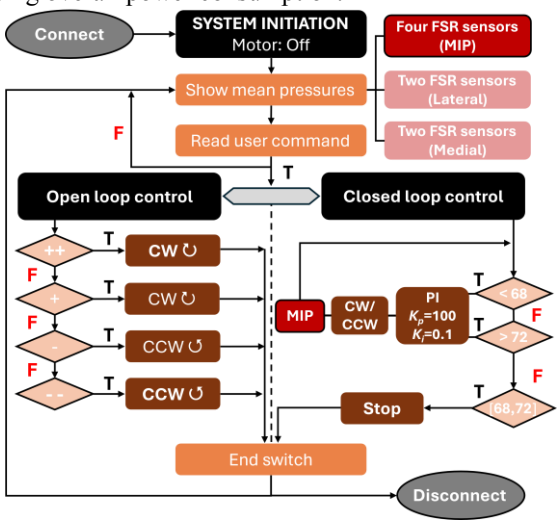

Fig. 3. Finite-state machine diagram of the control system implemented for socket volume regulation. After connection, the system initializes with the motor off and displays the Mean Interface Pressure (MIP) from four FSR sensors, including medial and lateral averages. The user can select either open- or closed-loop control: in open-loop, motor speed and direction are controlled via predefined buttons; in closed-loop, a PI controller maintains MIP within 70 ± 2 kPa using sensor feedback. F: False; T: True.

When automatic mode is activated, the system continuously monitors the MIP and drives the motor within a speed range of –195 rpm to +195 rpm (maximum CW and CCW speeds, respectively) to bring the MIP within the target deadband (i.e., 68 - 72 kPa). At each control cycle, the current MIP ($P_{PV}(t)$) is compared to the nearest band edge (P_{SP}), and the controller computes a control error, $e(t)$:

$$e(t) = P_{SP} - P_{PV}(t) \quad (2)$$

Based on this error, the motor speed is calculated using a standard PI control law:

$$u(t) = K_p e(t) + K_i \int_0^t e(t)dt \quad (3)$$

Where $u(t)$ is the instantaneous motor speed (bounded between ±195 rpm), with controller gains equal to $K_p = 100$ and $K_i = 0.1$. If MIP falls within the deadband, the controller sets the motor output to zero, and the socket volume remains constant. When pressure drops below 68 kPa, the motor retracts the cable at a dynamic rate by winding it onto the BOA dial spool, contracting the socket until MIP reaches the lower band edge. Conversely, when pressure exceeds 72 kPa, the motor releases the cable, expanding the socket smoothly until MIP approaches the upper threshold. Upon receiving the *Stop* command, the system stops the motor and exits automatic mode.

C. Experimental Setup

Experimental tests were conducted to verify the reliability, mechanical performance, and effectiveness of the proposed system, using experimental setups consistent with those reported in the literature [7], [9], [17], [21]. The high-fidelity in-vitro residual limb simulator (Fig. 1d), composed of silicone materials mimicking soft tissues and integrating a hydraulic chamber, was used to replicate realistic interface pressures and to assess both the cable tension force required to reach the target pressures as well as the socket's volumetric adaptability. During tests, the sensorized liner was worn on the simulator and inserted into the socket. Controlled volume fluctuations were achieved through water injection in the simulator hydraulic chamber using two syringe pumps (model NE-1010, New Era Pump Systems, Inc.), allowing up to +7.5% volume increment when 300 ml of water were injected, thereby reproducing physiological volume variation conditions in people with transfemoral amputation [4]. To assess the socket ability to withstand the required forces, a rigid mock residuum made of chalk and replicating the simulator's shape was used, with the liner positioned over it. The mock includes a stainless-steel rod to connect it to a 1 kN load cell of an Instron 5967 universal testing machine.

III. Results

A. Characterization tests

In characterization tests, the objective was to determine the cable displacement and force ranges required by the motor to reach the target MIP, across four different residual limb simulator volumes: V_0, V_0 +2.5%, V_0 +5%, V_0 +7.5%, where $V_0 = 3836.5 \pm 19.1$ cm^3. During testing, the adjustable socket system with the simulator was fixed in position without the actuation unit, and the two ends of the cable were pulled centrally using the Instron machine, until MIP exceeded the 70 kPa setpoint by ~10 kPa. Cable displacement and pulling force were recorded over seven cycles per volume condition, and results were averaged across cycles. To reach a pressure of 70 kPa, cable displacements of 6.41 ± 0.05 cm, 5.61 ± 0.03 cm, 3.50 ± 0.01 cm, and 2.11 ± 0.14 cm and corresponding pulling forces of 36.2 ± 0.2 N, 32.4 ± 0.2 N, 22.7 ± 0.4 N, and 4.8 ± 0.2 N were required at simulator's volumes V_0, V_0+2.5%, V_0+5%, V_0+7.5%, respectively (Fig. 4). The required cable tensions are significantly lower than the estimated maximum output of the actuation system (486 N), ensuring a FOS higher than 10, confirming the feasibility of proposed approach.

B. Mechanical tests

One of the most important requirements of the system is its ability to withstand the user's weight and the loads generated during walking. To prevent skin complications and secondary issues, the vertical displacement between socket and limb (i.e., pistoning) should be minimized as much as possible [30]. To assess this, the adjustable socket system was subjected to cyclic axial loading using Instron machine and rigid mock residuum. Tests were done according to the ISO 10328 preloading conditions and following protocols in literature [17], [31], [32].

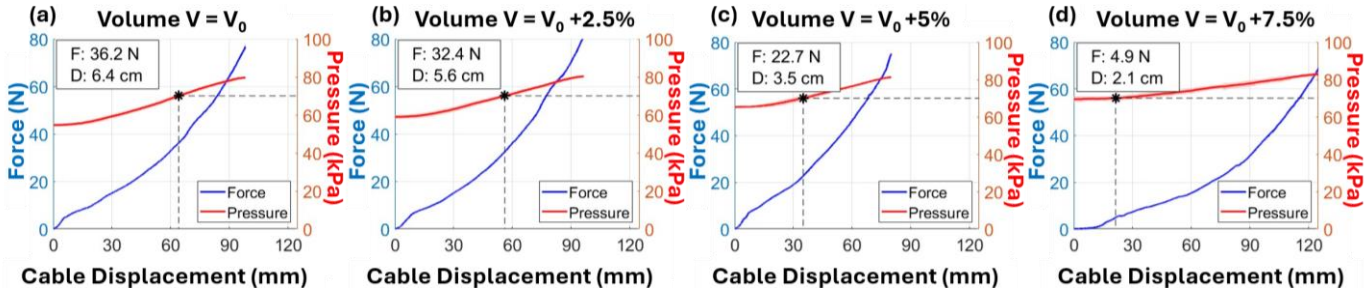

Fig. 4. Characterization tests results. Pressure and cable tension force (F) as a function of the cable displacement (D) for the adjustable socket on the in-vitro simulator at four different volumes: (a) V0, (b) V0 +2.5%, (c) V0 +5%, and (d) V0 +7.5%. Measurements were taken while pulling and thereby shortening the cable within the socket mechanism, continuing until the pressure exceeded the setpoint of 70 kPa by approximately 10 kPa. The asterisk indicates the displacement and force values corresponding to 70 kPa pressure. Total cable length 1150 mm.

Specifically, four different tensile loading conditions were applied to simulate gait phases, by cyclically loading and unloading the socket. Each set of cyclic tests began with a compressive preload of 800 N, followed by unloading the system to 700 N, 550 N, 300 N, and 150 N, corresponding to net tensile loads of 100 N, 250 N, 500 N, and 650 N, respectively. The tests were performed for three different socket adjustments, corresponding to cable shortenings of 0 mm, 30 mm, and 60 mm, relative to the total cable length of 1150 mm. For each condition, eleven load cycles were executed, and the vertical displacement was averaged across cycles. The observed maximum vertical displacements were: 5.77 ± 0.03 mm, 5.35 ± 0.01 mm, and 5.10 ± 0.01 mm for 0 mm, 30 mm, and 60 mm cable shortening, respectively (Fig. 5a, b, c). All measured values remained well below the 10 mm pistoning safety threshold commonly referenced in the literature for above-knee prostheses [30]. The consistently low displacement values across conditions demonstrate that the proposed system provides effective suspension, ensuring a stable interface thanks to the magnetic suspension and the customized socket shape, tailored to the geometry of the simulator. Although varying the socket pressure through cable adjustment would be expected to influence relative displacement, this effect was not clearly observed in our tests. This is likely due to the low friction coefficient between the silicone liner and the rigid plaster model, which limits the sensitivity of interfacial movement to pressure. However, when worn by a user, the higher friction between the liner and the skin is expected to further reduce relative vertical displacement between the socket and the residual limb. The use of a rigid and mechanically resistant mock residuum was necessary to safely apply the high loads required during testing, despite its inability to replicate the mechanical and tribological behavior of human soft tissue.

Subsequently, the mechanical robustness of the socket system, with particular focus on the 3D-printed distal attachment made of PEEK CA20, was assessed through dynamic and static load testing. A vertical compressive force of 900 N was applied to simulate the single-limb stance phase of a 90 kg user, which also corresponds to the maximum load attainable with the available testing apparatus. For dynamic testing, the system was subjected to 500 loading cycles of 900 N for each of the three cable configurations (0 mm, 30 mm, and 60 mm cable tightening), for a total of 1500 consecutive cycles. No cracks, deformations, or visible damage were observed, and the maximum displacement was 8.87 ± 0.18 mm, 7.44 ± 0.06 mm, and 6.43 ± 0.09 mm for 0 mm, 30 mm, and 60 mm cable shortening, respectively, below the 10 mm threshold and likely due to compression of the silicone liner at the distal end (Fig. 5d). For static testing, a sustained load of 900 N was applied for 20 minutes for each cable configuration. Again, the system showed no structural failure. These results confirm that the 3D-printed adjustable socket made of PA12 GB and the PEEK CA20 can safely withstand both dynamic and prolonged peak loads typical of daily prosthetic use.

C. In vitro validation

The ability of the proposed socket to autonomously regulate interface pressure in response to residual limb volume fluctuations was validated through in vitro experiments using the residual limb simulator (see Supplementary Video). The test was repeated five times. At the start of each trial, the simulator was at its baseline volume (V_0) and the socket in its resting configuration (0 mm cable shortening). The system measured an initial average MIP of 49.0 ± 1.9 kPa.

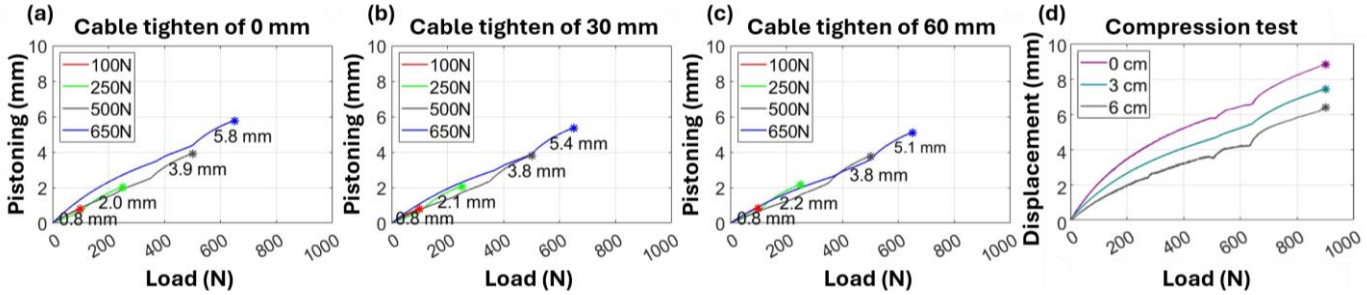

Fig. 5. Mechanical test results: vertical displacement (pistoning) under axial loads of 100 N, 250 N, 500 N, and 650 N, applied by unloading from an initial compressive preload of 800 N, for (a) 0 mm, (b) 30 mm, and (c) 60 mm cable tightening. (d) Vertical displacement under cyclic compressive loads ranging from 0 to 900 N over 500 cycles, shown for all three cable tightening conditions (0 mm, 30 mm, and 60 mm).

Upon activation of the closed-loop mode, the control unit autonomously tightened the cable via motor actuation until the pressure reached the lower edge of the control band (i.e., 68 kPa), corresponding to a cable shortening of 6.2 ± 0.2 cm. The closed-loop mode was then deactivated, and 300 ml of water were injected into the simulator to simulate a +7.5% volume increase, causing the MIP to rise to 86.3 ± 2.0 kPa. When the closed-loop mode was reactivated, the system responded by loosening the cable by 6.0 ± 0.3 cm, thereby restoring the pressure within the target deadband. These tests confirm the socket's ability to autonomously regulate interface pressure by tightening or loosening the cable with good reliability. However, small oscillations in pressure values (likely caused by sensor noise and the hyperelastic behavior of the silicone liner) were observed near the control band edges (i.e., 68 kPa and 72 kPa), resulting in slightly lower or higher measured interface pressures. Specifically, an average MIP of 67.9 ± 0.08 kPa was recorded during socket tightening, and 72.82 ± 0.10 kPa during socket enlargement, on the five tests.

IV. Discussion and Conclusions

This study presents a 3D-printed, volume-adjustable socket for above-knee prostheses, designed to address one of the ongoing clinical challenges: the need for dynamic adaptation to residual limb volume fluctuations. By combining additive manufacturing, sensing, and a hybrid motorized/manual control mechanism, the proposed solution enables effective modulation of the socket volume, ensuring a proper fit and appropriate pressure on residual limb tissues. In addition to its functional advantages, the use of 3D printing enables on-site fabrication of the socket without the need for specialized prosthetic laboratories or the equipment typically required for traditional lamination processes. This significantly reduces production costs and streamlines manufacturing. From both an environmental and occupational health perspective, 3D printing also offers important benefits by minimizing material waste and reducing clinicians' exposure to harmful chemicals and fine dust commonly associated with carbon fiber reinforced resin-based fabrication. Thanks to the optimized selection of 3D-printable materials, the socket offers an excellent compromise between mechanical strength and lightness. Indeed, static and dynamic load tests up to 900 N confirmed the structural integrity of the 3D-printed socket, made of PA12 GB with a PEEK CA20 distal attachment. Although some studies have used higher load levels as defined for the P6 activity level of ISO 10328, socket mechanical behavior is dominated by pressure distribution, shear, and interaction with soft tissues, rather than by large axial loads transmitted through rigid components. As a result, the loading conditions, failure modes, and clinical requirements of sockets differ fundamentally from those addressed in ISO 10328, which was developed specifically for evaluating the structural performance of lower-limb prosthetic components like feet, ankles, pylons, and knee mechanisms. This mismatch is also an element of active discussion within the research community, as no dedicated standard for the mechanical behavior of sockets is currently available [33]. Thus, the socket can withstand the loads generated during walking, while weighing only 1 kg, which is comparable to traditional carbon fiber sockets, lighter than other 3D-printed sockets (~1.2-1.6 kg [17] [19]) and 20–30% lighter than prefabricated adjustable commercial sockets, such as Ottobock Varos (1.3 kg) and Ossür Connect TF (1.5 kg). The total system including motor, gears, battery, and electronic control board, weights 2.2 kg. However, the system exhibits a high safety factor: it can generate 486 N, nearly 10 times more than the 36 N required to reach the target interface pressure, indicating that future designs could adopt a smaller and lighter motor–transmission assembly to reduce size, power consumption, and overall weight, while still providing sufficient torque and reliability. For example, pulley-based actuation could reduce weight and bulk compared to traditional gear-based systems. Alternatively, custom 3D-printed gears using high-performance polymers (e.g., nylon or fiber-reinforced composites) may offer an effective trade-off between weight, strength, precision, and customization potential [34]. Moreover, 3D printing could enable further weight reduction of the entire structure using lattice architectures, which may also enhance mechanical performance, material efficiency, and heat dissipation. Previous research has shown that ±2.5 kg changes in prosthetic mass have limited impact on gait parameters or muscular effort, especially when the added weight is located proximally [35]. Based on this, a socket weight of 2.2 kg falls within an acceptable range and is unlikely to negatively affect walking performance. Additionally, while heavier than passive systems, the proposed solution integrates active control in both open- and closed-loop configurations, along with embedded pressure sensing, while still allowing easy switching to manual volume adjustment in passive mode, all within a personalized 3D-printed structure. By providing feedback on the pressure applied to residual limb tissues, the proposed solution helps prevent excessive skin stresses that could lead to discomfort or injury, an aspect often overlooked in passive systems. Compared to other active systems, such as the device by Paternò et al. [31], the proposed design offers approximately a 20% weight reduction and a more compact form factor, with the actuation unit integrated into the socket structure, improving wearability from multiple perspectives. Compared to pneumatic solutions like the socket by Lee et al. [8], our system offers a more uniform pressure distribution, improved stability and it can achieve interface pressures more than twice (≈70 kPa vs. 27 kPa). Pneumatic systems inherently suffer from air compressibility and pressure losses under load, leading to higher pistoning, more frequent activations, and consequently increased power consumption despite having comparable average current draw (0.3 A in our system, 0.2 A in pneumatic socket [8]. On the contrary, the motorized cable-driven actuation of our system ensures firmer support and reduces relative movement, particularly under dynamic gait conditions, as confirmed by mechanical tests showing vertical displacement below 6 mm, well within the safety threshold reported in the literature [30], and lower than pneumatic solutions [8]. The results validated the effectiveness of the integrated magnetic suspension system, which provides a more compact alternative to pin-lock mechanisms. Even lower displacements are expected in real use, thanks to the higher friction between silicone liner and user's skin compared to that between silicone and the rigid mock residuum. Characterization tests showed that the socket needs moderate cable tensions

(max 36.2 ± 0.2 N) to maintain interface pressure within a clinically relevant range across varying simulated limb volumes, well within the mechanical limits generated by the motor and the transmission mechanism with the BOA® dial (theoretically calculated of 486 N). The socket demonstrated its ability to maintain pressure within the target range of 70 ± 2 kPa in vitro. This range was chosen based on clinical literature, but future versions could employ patient-specific target pressures prescribed by the prosthetist, based on individual anatomical and clinical characteristics, to further enhance fit and comfort. The FSR sensors were chosen for their thin, flexible, and low-cost design, enabling simple integration, and making them suitable for demonstrating the feasibility of the smart socket. Although not intended for highly accurate absolute pressure measurements, FSRs can reliably detect relative pressure changes under consistent mechanical conditions, which is sufficient for the closed-loop control used here [28]. Sensor number, placement, and thresholds will be optimized, potentially using redundancy-reduction methods to identify the minimal sensing configuration needed for effective control [36]. Future iterations will also investigate more robust technologies to improve long-term sensitivity, and reliability in both static and dynamic measurements. A promising alternative could be offered by recent work from Ballesteros et al. [37], who introduced inductive distance sensors. These sensors offer the potential for more robust measurements, being less susceptible to disturbances and artifacts generated during gait.

Additional future work will investigate more advanced control strategies, including adaptive and model-based approaches, to further improve the robustness and responsiveness of the volume-regulation system. Finally, a pilot study with 3-5 unilateral transfemoral users will be conducted under ethical approval. Participants will evaluate the smart socket mounted on their own prosthesis, allowing direct comparison with their usual baseline socket. The protocol will include static fitting, standing balance, and short supervised indoor walking trials, during which basic gait parameters (step symmetry, stride time, walking speed), user-reported comfort and stability will be assessed. Safety will be ensured through clinician supervision, predefined stop criteria, and the presence of an emergency-stop function integrated into the system.

ACKNOWLEDGMENT

The authors gratefully acknowledge the support of BOA® Technology Inc., SelleRoyalGroup, and MADEINADD s.r.l. for providing components and technical insights.

REFERENCES

[1] K. Ziegler-Graham, *et al.*, 'Estimating the Prevalence of Limb Loss in the United States: 2005 to 2050', *Arch. Phys. Med. Reh.*, vol. 89, no. 3, 2008.
[2] S. Manz, *et al.*, 'A review of user needs to drive the development of lower limb prostheses', *J. NeuroEngineering Rehabil.*, vol. 19, no. 1, p. 119, 2022.
[3] C. Putz, *et al.*, 'Structural changes in the thigh muscles following trans-femoral amputation', *Eu. J. Orth. Surg. Traum.*, vol. 27, pp. 829–835, 2017.
[4] L. Paternò, *et al.*, 'Residual limb volume fluctuations in transfemoral amputees', *Sci. Rep.*, vol. 11, no. 1, p. 12273, 2021.
[5] R. Gailey, 'Review of secondary physical conditions associated with lower-limb amputation and prosthesis use', *J. Reh. Res. Dev.*, vol. 45, no. 1, 2008.
[6] M. Baldock, *et al.*, 'Adjustable prosthetic sockets: a systematic review of industrial and research design characteristics and their justifications', *J. NeuroEngineering Rehabil.*, vol. 20, no. 1, p. 147, 2023.
[7] J. H. Seo, *et al.*, 'A Prosthetic Socket with Active Volume Compensation for Amputated Lower Limb', *Sensors*, vol. 21, no. 2, p. 407, 2021.
[8] K. H. Lee, *et al.*, 'A Pneumatically Controlled Prosthetic Socket for Transfemoral Amputees', *Sensors*, vol. 24, no. 1, p. 133, 2023.
[9] R. Z. Gao, *et al.*, 'Soft Dynamic Fluidic Cushion for Pressure Sore Management in Transtibial Prosthetics – A Proof-of-Concept Study', *IEEE TBME*, pp. 1–14, 2025.
[10] C. J. Gurrey, *et al.*, 'Socket release/relock: An innovative mechanism to maintain residual limb volume', *Med. Eng. Phys.*, vol. 90, pp. 100–106, 2021.
[11] J. E. Sanders, *et al.*, 'A motor-driven adjustable prosthetic socket operated using a mobile phone app: A technical note', *Med. Eng. Phys.*, vol. 68, 2019.
[12] 'Varos | Varos Socket | Socket Technologies / Liners | Lower Limb Prosthetics | Prosthetics | Ottobock US Shop'. Accessed: Dec. 18, 2024. [Online]. Available: https://shop.ottobock.us/Prosthetics/Lower-Limb-Prosthetics/Socket-Technologies-Liners/Varos-Socket/Varos/p/5A60
[13] 'Connect® TF Adjustable Socket for Low Active TF Amputees. Ossur.com'. Accessed: Dec. 18, 2024. [Online]. Available: https://www.ossur.com/en-us/prosthetics/sockets/connect-tf
[14] A. Nia, *et al.*, 'Evaluation of the new, patient-adjustable socket system Varos in the early phase of prosthetic rehabilitation: a pilot study', *Eur. J. Phys. Rehabil. Med.*, vol. 58, no. 3, 2022.
[15] J. E. Sanders, S. Fatone, 'Residual limb volume change: Systematic review of measurement and management', *J. Rehabil. Res. Dev.*, vol. 48, no. 8, 2011.
[16] R. Safari, Lower limb prosthetic interfaces: Clinical and technological advancement and potential future direction. *J. Prosth. Ort.* 2020; vol. 44, no. 6.
[17] B. Pousett, *et al.*, 'An investigation of the structural strength of transtibial sockets fabricated using conventional methods and rapid prototyping techniques', *Can. Prosthet. Orthot. J.*, 2019.
[18] C. Matsika Klossa, *et al.*, 'Tensile properties of 3D printed carbon fiber reinforced nylon specimens', *Mater. Today Proc.*, vol. 93, pp. 571–574, 2023.
[19] E. Nickel *et al.*, 'Pilot Test of a Definitive Prosthetic Socket Made with 3D Printing Technology', *J. Prosthet. Orthot.*, vol. 35, no. 1, pp. 55–60, 2023.
[20] K. T. Nguyen, L. Benabou, and S. Alfayad, 'Systematic Review of Prosthetic Socket Fabrication using 3D printing', in *Proceedings of the 2018 4th International Conference on Mechatronics and Robotics Engineering*, Valenciennes France: ACM, 2018, pp. 137–141.
[21] E. A. Nickel, *et al.*, 'Strength Testing of Definitive Transtibial Prosthetic Sockets Made Using 3D-Printing Technology', *JPO* vol. 32, no. 4, 2020.
[22] T. Marinopoulos, S. Li, and V. V. Silberschmidt, 'Structural integrity of 3D-printed prosthetic sockets: Experimental study for paediatric applications', *J. Mater. Res. Technol.*, vol. 24, pp. 2734–2742, 2023.
[23] 'BOA® Fit System'. Accessed: Dec. 18, 2024. [Online]. Available: https://www.ossur.com/en-us/prosthetics/sockets/connect-tf
[24] 'MadeInAdd | Produzione on-demand: Stampa 3D, CNC'. Accessed: July 10, 2025. [Online]. Available: https://www.madeinadd.com/it
[25] B. I. Oladapo, *et al.*, '3D printing of PEEK and its composite to increase biointerfaces as a biomedical material- A review', *Colloids Surf. B Biointerfaces*, vol. 203, p. 111726, 2021.
[26] J. R. Sarot, *et al.*, 'Evaluation of the stress distribution in CFR-PEEK dental implants by the three-dimensional finite element method', *J. Mater. Sci. Mater. Med.*, vol. 21, no. 7, pp. 2079–2085, 2010.
[27] W. Flanagan *et al.*, 'Prosthetic Limb Attachment via Electromagnetic Attraction Through a Closed Skin Envelope', *IEEE TBME*, vol. 71, no. 5, 2024.
[28] E. C. Swanson, *et al.*, 'Evaluation of Force Sensing Resistors for the Measurement of Interface Pressures in Lower Limb Prosthetics', *J. Biomech. Eng.*, vol. 141, no. 10, p. 101009, 2019.
[29] L. Paternò, *et al.*, 'Quantitative analysis of interface pressures in transfemoral prosthetic sockets', *Prosthet. Orthot. Int.*, vol. 48, no. 2, 2024.
[30] A. Eshraghi, *et al.*, 'Pistoning assessment in lower limb prosthetic sockets', *Prosthet. Orthot. Int.*, vol. 36, no. 1, pp. 15–24, 2012.
[31] L. Paternò *et al.*, 'Smart Transfemoral Prosthetic Socket with Motorized Cable-Driven System', *Adv. Intell. Syst.*, p. 2400995, 2025.
[32] J. Quinlan, *et al.*, 'Using mechanical testing to assess the effect of lower-limb prosthetic socket texturing on longitudinal suspension', *PLOS ONE*, vol. 15, no. 8, p. e0237841, 2020.
[33] A. Dickinson *et al.*, 'Toward standardized methods for prosthetic socket mechanical testing', *Prosthet. Orthot. Int.*, vol. 47, no. 1, pp. 1–2, 2023.
[34] L. Pujari, *et al.*, 'Recent advancements in 3D printing for gear design and analysis: a comprehensive review', *Multiscale Multidiscip. Model. Exp. Des.*, vol. 7, no. 6, pp. 4979–5003, 2024.
[35] R. Selles, Weighing weight: effect of below-knee prosthetic inertial properties on gait. 2002 Sep 18.
[36] Z. Wenyao, et al. 'Redundancy reduction for sensor deployment in prosthetic socket: A case study.' Sensors 22, no. 9 (2022): 3103.
[37] D. Ballesteros *et al.*, 'Fabricating Sockets with Distance Sensors for Monitoring Prosthesis Use and Socket Fit', *J. Prosth. Orth.*, vol. 36, no. 2, 2024.